Structure and magnetic properties of $LaMn_{1-x}Mg_xO_3$ compounds

J. Blasco,* J. García, G. Subías, and M. C. Sánchez
Instituto de Ciencia de Materiales de Aragón and Departamento de Física de la Materia Condensada, Consejo Superior de Investigaciones Científicas y Universidad de Zaragoza, 50009 Zaragoza, Spain
(Received 19 January 2004; revised manuscript received 26 April 2004; published 29 September 2004)

We substitute Mg for Mn in the $LaMnO_3$ compound. $LaMn_{1-x}Mg_xO_3$ single phases can be formed up to $x=0.5$. Structural and electronic properties were studied by means of x-ray diffraction and x-ray absorption spectroscopy. A double perovskite is observed for $x \geqslant 0.4$ whereas no long Mn/Mg ordering is detected for $x \leqslant 0.3$. The former samples also show a structural transition from rhombohedral to monoclinic with decreasing temperature. The local structure around Mn evidences the absence of Jahn-Teller distortion since $x=0.1$. The samples with low Mg content have a ferromagnetic ground state while samples with $x \geqslant 0.3$ undergo a spin-glass transition at low temperatures. The frequency dependence of the freezing temperature follows a Vogel-Fulcher law and it is similar to canonical spin-glasses. The high temperature ac susceptibility of all samples obeys the Curie-Weiss law but the effective paramagnetic moments do not agree with a spin-only contribution for $x \leqslant 0.4$. Finally, we have demonstrated that Mg does not replace La in the perovskite lattice by studying selected $La_{1-x}Mg_xMnO_3$ samples. It always enters onto the perovskite B-site.

DOI: 10.1103/PhysRevB.70.094426 PACS number(s): 75.47.Lx, 61.10.Ht, 61.66.Fn, 75.10.Nr

I. INTRODUCTION

A large effort has been devoted to the study of mixed oxides of rare earth and Mn, the so-called manganites, since the discovery of giant magnetoresistance.[1] Nevertheless, the large variety of properties shown by manganites is not completely understood so far. A way to gain insight into the physical properties of these compounds lie in the replacement of Mn in the parent compound, $LaMnO_3$. For instance, the homovalent substitution of Mn^{3+} by Ga^{3+} is detrimental for the antiferromagnetic ordering of $LaMnO_3$ and $LaMn_{0.5}Ga_{0.5}O_3$ is ferromagnetic at low temperatures.[2] This magnetic change is correlated with the continuous disappearing of static Mn^{3+} Jahn-Teller distortion.[3] Now, we want to focus on the effect of disorder in the Mn sublattice with mixed valency. This topic has been addressed by replacing Mn with other 3-*d* transition metals in $La_{2/3}Ca_{1/3}MnO_3$ but it is difficult to separate disorder effects from new magnetic interactions. Normally, such a substitution is detrimental of both the ferromagnetic interaction and metallic conductivity.[4,5] This is true even for nonmagnetic elements[6] such as Zn^{2+}. Here we show an alternative way to study the role of disorder in these compounds by introducing Mg^{2+} into the Mn sublattice of $LaMnO_3$. $LaMn_{1-x}Mg_xO_3$ samples were the subject of several studies. Blasse in the 1950s claimed that Mn and Mg are ordered onto the B-site in the $LaMn_{0.5}Mg_{0.5}O_3$ compound forming a double perovskite[7] but the exact crystallographic structure has not been refined so far. Recent surveys on these compounds have mainly been focused on their catalytic properties.[8] The electrical properties of $LaMn_{1-x}Mg_xO_3$ ($x \leqslant 0.2$) were also studied showing that electrical resistivity decreases with *x* but they keep on being semiconducting though the samples are ferromagnets.[9] Moreover, they exhibit a large nonlinear conduction at low field strengths in the ferromagnetic phase.[10]

Our aim in this work is twofold. First, we have carried out the structural and electronic characterization of the series verifying the existence of a double perovskite at $x \sim 0.5$. Second, we have characterized the magnetic properties of this series establishing relationships with structural and electronic properties. In particular, the comparison of the properties exhibited by this series to related manganites was also a matter of our interest.

Finally, recent papers claim for the substitution of Mg for La.[11–14] These authors report that the large orthorhombic distortion induced by this replacement leads to insulating ferromagnetic samples with an undisturbed Mn sublattice. This surprising result has also deserved our attention in order to establish properly the properties of the La-Mg-Mn-O system.

II. EXPERIMENTAL

The compounds $LaMn_{1-x}Mg_xO_3$ ($x=0.1,0.2,0.3,0.4,0.5$) were prepared by ceramic procedures. Stoichiometric amounts of La_2O_3, $MnCO_3$ and MgO were mixed, grounded and heated at 900 °C overnight. Then, the powders were pressed into pellets and sintered, with intermediate grindings, at 1400 °C for 1 *d* in air. The pellets were reground, repressed and sintered at 1500 °C for 2 *d* with intermediate regrinding. This step was performed in air for $x \leqslant 0.2$ and in an oxygen current flow for $x \geqslant 0.3$ to ensure the adequate oxygen stoichiometry for the latter.

All samples were characterized by x-ray powder diffraction at room temperature. All x-ray patterns were indexed as an orthorhombic perovskite single phase for $x \leqslant 0.3$ whereas $x=0.4$ and $x=0.5$ showed two perovskite phases (orthorhombic-like and rhombohedral) at room temperature. Measurements at low temperature were also performed for $x=0.4$ and $x=0.5$ by coupling an Oxford Instruments cryostat to the diffractometer.

Step-scanned powder diffraction patterns were collected at room temperature using a D-max Rigaku system with a rotating anode. The diffractometer was operated at 100 mA and 40 kV with a Cu anode. A graphite monochromator was

used to select the Cu Kα radiation. Data were collected from 19º up to 130º with a step size of 0.02º and a counting rate of 5 sec/step. The crystal structures were refined by the full pattern method using the Fullprof program.[15]

X-ray-absorption measurements at the Mn K-edge were carried out at the BM29 beam line at the European Synchrotron Radiation Facility (Grenoble, France). A fixed-exit Si(111) double-crystal monochromator with an estimated energy resolution of $\Delta E/E=8\times10^{-5}$ was used. The absorption spectra were recorded in the transmission mode at room temperature using ionization chambers as detectors. A Mn foil was simultaneously measured at room temperature for energy calibration. X-ray absorption near edge structure (XANES) spectra were normalized to the high part of the spectrum (around 100 eV above the absorption edge) after a linear background subtraction. Extended x-ray absorption fine structure (EXAFS) spectra $[\chi(k)]$ were obtained by removing the smooth atomic absorption coefficient (μ_0) by means of a cubic spline fit. The Fourier Transform (FT) of the *k*-weighted EXAFS spectra was calculated between 3.0 and 12.0 Å^{-1} using a Gaussian window. The EXAFS spectra were analyzed using the FEFFIT package[16] to obtain Debye-Waller factors (DW) and the inter-atomic distances. FEFFIT uses backscattering amplitudes and phases calculated by the FEFF 8.10 code[17] for the individual scattering paths. The structural analysis was performed in the *R*-space fitting mode up to 2.2 Å. The model used to fit the first shell Mn K-edge data takes into account only Mn-O single scattering paths.

The oxygen content of the samples was determined from redox titration by using Mohr's salt and $KMnO_4$. Only the sample with $x=0.1$ showed a significant excess of oxygen, i.e., a defect of cations.[18] The rest of the samples can be considered oxygen stoichiometric within the experimental error. Table I summarizes the structural parameters at room temperature and oxygen content for all studied samples.

Magnetic measurements were performed between 5 and 380 K and up to 5 T in a commercial Quantum Design (SQUID) magnetometer provided with an ac experimental set-up.

TABLE I. Structural parameters for $LaMn_{1-x}Mg_xO_{3+\delta}$ samples at 300 K. The oxygen content is given as δ, space group, lattice parameters, fractional coordinates, isotropic displacement factors (B) and reliability factors (defined as Ref. 15). Mn and Mg occupations at (1/200) for $x\leqslant0.3$ were fixed to $1-x$ and x, respectively. An only B-factor accounts for the oxygens in these samples. (*) The occupation for this site was fixed to 0.1 Mn+0.4 Mg. The $x=0.4$ and 0.5 also present the minoritary low-temperature phase whose amount can be deduced from the second line (s.g.).

Sample	$x=0.1$	$x=0.2$	$x=0.3$	$x=0.4$	$x=0.5$
δ	0.11	0.03	0.01	0.02	−0.01
s.g.	*Pbnm*	*Pbnm*	*Pbnm*	$R\bar{3}$(79%)	$R\bar{3}$(91%)
a (Å)	5.5339(1)	5.5340(1)	5.5288(1)	5.5156(1)	5.5109(1)
b (Å)	5.4948(2)	5.5002(1)	5.4898(1)	-	-
c (Å)	7.7844(2)	7.7912(2)	7.7771(2)	13.2977(2)	13.2861(2)
La:x	0.9966(3)	0.9951(2)	0.9947(2)	0	0
y	0.0191(1)	0.0210(1)	0.0179(1)	0	0
z	1/4	1/4	1/4	0.2494(2)	0.2498(1)
B (Å^2)	0.34(2)	0.18(1)	0.46(2)	0.34(2)	0.45(2)
Mn:*x y z*	1/2 0 0	1/2 0 0	1/2 0 0	0 0 0	0 0 0
B (Å^2)	0.05(2)	0.09(2)	0.35(3)	0.15(10)	0.38(9)
Mg:*x*,*y*,*z*	1/2 0 0	1/2 0 0	1/2 0 0	0 0 1/2*	0 0 1/2
B (Å^2)	0.05(2)	0.09(2)	0.35(3)	0.10(10)	0.25(10)
O:x	0.081(2)	0.071(2)	0.043(1)	0.556(1)	0.559(1)
y	0.492(1)	0.490(1)	0.496(1)	0.010(2)	0.011(2)
z	1/4	1/4	1/4	0.2552(7)	0.2521(5)
O:x	0.723(1)	0.725(1)	0.731(1)	-	-
y	0.275(2)	0.276(1)	0.268(1)	-	-
z	0.030(1)	0.0351(8)	0.0462(8)	-	-
B (Å^2)	0.86(12)	0.89(11)	0.44(9)	0.38(12)	0.52(9)
R_p/R_{wp} (%)	7.4/10.8	6.6/9.5	7.0/9.7	6.4/9.0	6.1/9.0
R_{Bragg} (%)	3.1	3.4	4.2	3.3	3.0

III. RESULTS AND DISCUSSION

According to the literature,[7–14] Mg^{2+} can replace both La and Mn sites, following similar synthetic routes. This point should be clarified before starting the study of the La-Mg-Mn-O system. The appendix is devoted to the existence of $La_{1-x}Mg_xMnO_3$ compounds. We advance that such samples are composed by several phases and Mg^{2+} only enters onto the perovskites B-site. Therefore, we are now focusing on the study of the $LaMn_{1-x}Mg_xO_3$ series.

A. Crystal structure

Figure 1 shows a detail of the x-ray patterns at room temperature for $LaMn_{1-x}Mg_xO_3$ samples. Only $LaMn_{0.5}Mg_{0.5}O_3$ showed a tiny impurity of MgO, hard to notice in the pattern. The rest of the samples showed clear single phases. $LaMn_{1-x}Mg_xO_3$ belongs to the family of perovskite oxides, ABO_3, A being the large cation 12-fold coordinated (La in our case) whereas B-site is occupied by a small cation surrounded by 6 oxygens (Mn and Mg).

The patterns for $x\leqslant0.3$ can be indexed in an orthorhombic cell typical of a large amount of perovskites such as $GdFeO_3$. Therefore, these patterns were refined using the *Pbnm* space group. The refined structural parameters are summarized in Table I. A first glance to the patterns of $x\geqslant0.4$ samples suggests a rhombohedral structure as observed in related perovskites such as $LaNiO_3$. However, there is an additional peak (indicated by an arrow in Fig. 1) that cannot be indexed in the usual rhombohedral cell (space group $R\bar{3}c$). The presence of this superstructure peak is usually related to the atomic ordering onto the B-sites giving rise to a double perovskite. It was observed for $x=0.5$ in the past[7] but no crystallographic structure has been reported so far. We were successful in refining a related ordered structure in the $LaNi_{1-x}Mn_xO_3$ system using the space group $R\bar{3}$.[19] The assignation of $R\bar{3}$ is in agreement with recent calculations for ordered rhombohedral cells.[20] Therefore, we have refined the patterns for $x\geqslant0.4$ samples using this space group. However, the fits were not satisfactory enough and the detailed analysis

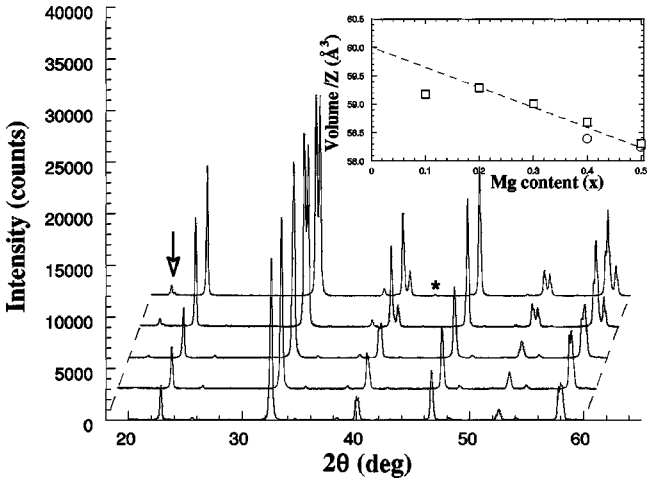

FIG. 1. Details of the x-ray patterns at room temperature for $LaMn_{1-x}Mg_xO_3$ samples. The patterns are shifted to right and upwards from bottom ($x=0.1$) to top ($x=0.5$) for the sake of comparison. Asterisk marks the tiny impurity of MgO. An arrow indicates the main superstructure peak ascribed to the Mn/Mg ordering. **Inset:** Evolution along the $LaMn_{1-x}Mg_xO_3$ series of the volume per chemical formula. Note that circles and squares refer to the rhombohedral and monoclinic phases, respectively, for $x=0.4$ and 0.5. The broken line indicates the slope of the hypothetical cubic cell whose edge varies from Mn^{3+}-O-Mn^{3+} to Mn^{4+}-O-Mg^{2+}.

of the patterns showed that these samples are composed by two perovskite phases at room temperature: The main $R\bar{3}$ phase and a minority orthorhombic-like phase. This fact could be due either to a phase segregation arising from a chemical inhomogeneity or to a structural phase transition at around room temperature as occurs in related systems.[21] In order to ascertain it, we have carried out x-ray diffraction measurements from 77 up to 330 K. $LaMn_{0.6}Mg_{0.4}O_3$ and $LaMn_{0.5}Mg_{0.5}O_3$ showed single orthorhombic-like phases at 77 K. Figure 2 compares x-ray patterns of both phases for $x=0.5$. According to Woodward,[20] there is not double perovskite with an (centrosymmetrical) orthorhombic lattice so these patterns were analyzed using the monoclinic $P2_1/n$ space group (subgroup of *Pbnm*) though β was practically 90º in all cases. Then, the patterns of $x \geqslant 0.4$ samples at room temperature were analyzed using a mixture of $R\bar{3}$ and $P2_1/n$ phases giving rise to accurate fits (see Table I). It is noteworthy that the first superstructure peak (the arrow in Fig. 1) is allowed for the *Pbnm* phase though its intensity is very low (see patterns of $x=0.1$ and 0.2 in Fig. 1). The pattern of $LaMn_{0.7}Mg_{0.3}O_3$ instead showed a significant intensity of this peak so that we have also refined it in $P2_1/n$. The new fits did not show any noticeable improvement respect to that of the previous refinement in *Pbnm*. Nevertheless, a partial ordering of cations onto the B-sites cannot be definitely discarded for this composition and a study on single-crystals would be desirable to shed light on this subject.

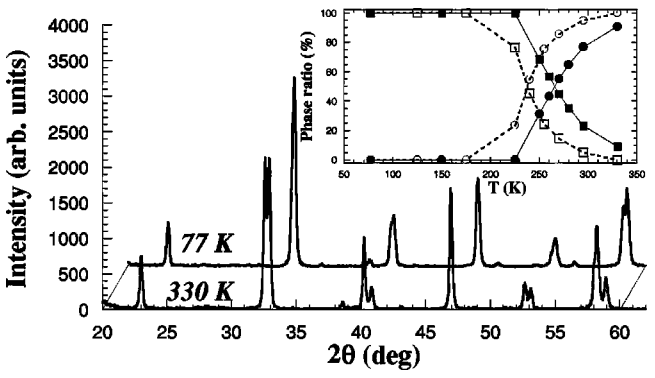

FIG. 2. Details of the *x*-ray pattern for $LaMn_{0.5}Mg_{0.5}O_3$ at 77 and 330 K. **Inset:** Thermal evolution of the phase ratio for $LaMn_{0.6}Mg_{0.4}O_3$ (black symbols) and $LaMn_{0.5}Mg_{0.5}O_3$ (white symbols). Circles refer to the rhombohedral phase while squares refer to the monoclinic phase.

Geometrical factors can account for the change from the orthorhombic to the rhombohedral cell along the $LaMn_{1-x}Mg_xO_3$ series. It is well known that the crystal structures of ABO_3 perovskites are related to the Goldschmidt tolerance factor defined as $t=(R_A+R_O)/[2^{1/2}(R_B+R_O)]$, R_A, R_B and R_O being the ionic radius for A, B and oxygen atoms, respectively. Values of *t* close to 1 are obtained for the ideal cubic perovskite while smaller values of *t* lead to cooperative tilting of the BO_6 octahedra in order to minimize the left space due to the A/B size mismatch.[22] Values of *t* slightly lower than 1 lead to the appearance of the rhombohedral unit cell ($a^-a^-a^-$ tilt system, following Glazer's notation[22]) whereas orthorhombic cells are observed for *t* significantly smaller than 1 ($a^+b^-b^-$ tilt system). The *t* value limiting rhombohedral and orthorhombic cells at room temperature seems to be located at $x\sim 0.4$ for this series. The trend observed in the $LaMn_{1-x}Mg_xO_3$ series, with the same A (La) atom for all samples suggests that the size of the B-site decreases with increasing the content of Mg. This counterintuitive finding can be understood in terms of the tabulated ionic radii[23] for six-coordinated Mn^{3+} (high-spin), Mn^{4+} and Mg^{2+} that are 0.645, 0.53 and 0.72 Å, respectively. According to an ionic picture as a first approximation, the replacement of a Mn^{3+} by a Mg^{2+} implies the oxidation of a second Mn^{3+} into Mn^{4+} to preserve the oxygen stoichiometry. Therefore, the full process can be viewed as the substitution of two Mn^{3+} by the mixture of Mn^{4+} and Mg^{2+}, resulting in a diminution of the average B-sublattice due to the small Mn^{4+} size. This feature can be better noted in the inset of Fig. 1 where the volume per formula unit is plotted for the whole series. Overall, this volume decreases following the expected decreasing of the average BO_6 octahedron. The only exception is observed for the $x=0.1$ sample that shows a smaller volume. This result can be ascribed to the large oxygen excess detected for this sample that entails the presence of cationic vacancies.[18] It is easy to realize that the rhombohedral cell has the smallest volume in samples where two phases coexist at room temperature ($x\geqslant 0.4$) so that a volume expansion with decreasing temperature, coupled to the structural transition, can be inferred for both samples as occurs in related systems.[21] Finally, the ratio of the $R\bar{3}$ phase increases with increasing *x* at room temperature. The inset of Fig. 2 shows the ratio of both phases for $x\geqslant 0.4$ samples as a function of temperature. The phase transition begins at lower temperature for $x=0.5$ and it is not complete at 330 K (high limit of our experimental set-up) for $x=0.4$.

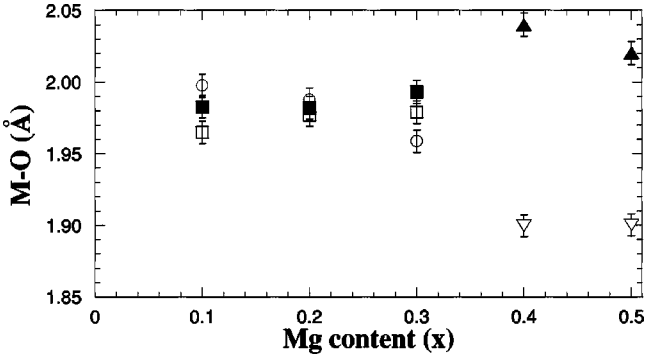

FIG. 3. Evolution along the $LaMn_{1-x}Mg_xO_3$ series of the M-O distance (M=Mn, Mg). Circles refer to M-O_{axial}, squares to M-$O_{equatorial}$, white triangles to Mn-O and black triangles to Mg-O.

An important structural result concerns to the Mg/Mn ordering onto the B-sites. This type of ordering is observed in perovskites when two atoms placed on the B-site have significant differences in either ionic size or valency state. The ordered arrangement of B-atoms gives rise to the so-called double perovskite $A_2BB'O_6$.[24] Our results show that $LaMn_{0.5}Mg_{0.5}O_3$ is actually a double perovskite, i.e., La_2MnMgO_6, and the ordering is preserved at least, down to $x=0.4$. Figure 3 shows the variation of B-O distances. The BO_6 octahedron shows a minor spread of B-O distances typical of the O-orthorhombic phase (samples with $x\leqslant 0.3$). The lack of tetragonal distortion in the MnO_6 octahedra can be ascribed to the oxidation of the Mn sublattice as occur in related manganites.[25,26] It is well known that a just perfect $Mn^{3+}O_6$ net is necessary to form the O′-orthorhombic structure.[3,27] In the case of the $x=0.1$ sample, the large oxygen excess also contributes to the oxidation of Mn. The samples with a high content of Mg exhibit two different BO_6 octahedra. The biggest corresponds to $Mg^{2+}O_6$ with an average Mg-O distance of ~2.03 Å whereas the Mn-O distance values ~1.90 Å. These data compare quite well to the tabulated ionic radii.[23]

B. Local electronic and geometrical structure

In order to gain insight into the electronic configuration and the local structure along this series, we have measured x-ray absorption spectra at the Mn K-edge at room temperature. Figure 4 shows the XANES spectra of the $LaMn_{1-x}Mg_xO_3$ samples compared to the reference compounds, $LaMnO_3$ (octahedral Mn^{3+}) and $CaMnO_3$ (octahedral Mn^{4+}). The XANES spectra for $LaMn_{1-x}Mg_xO_3$ show a strong resonance at energies (measured at the first inflection point) ranging between 6550.9 ($x=0$) and 6554.5 eV ($x=0.5$). The main difference among the spectra concerns to the position of this resonance (absorption edge). There is a continuous shift towards higher energies with increasing the Mg-content of the sample. The energy shift of the edge relative to Mn metal is collected in Table II. This shift can be correlated to the formal Mn valency (i.e., chemical shift). The edge for $x\leqslant 0.4$ samples lies at intermediate positions between $CaMnO_3$ and $LaMnO_3$, confirming a mixed valence state for the Mn atoms. The edge position for $x=0.5$ instead

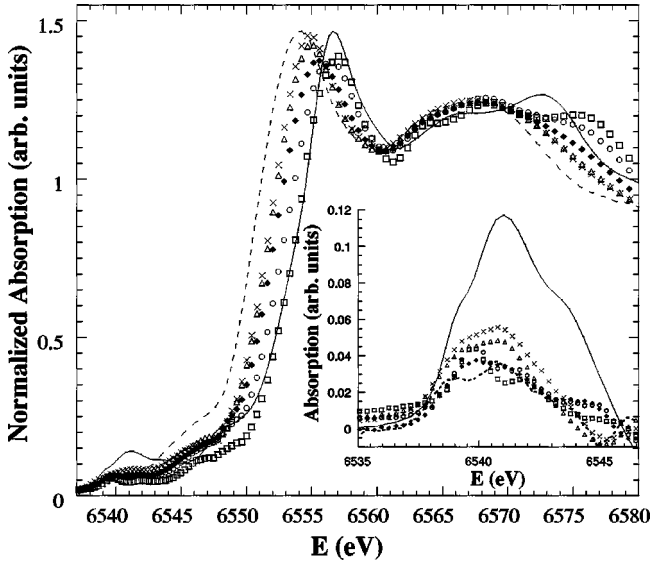

FIG. 4. Mn K-edge XANES spectra for $LaMnO_3$ (broken line), $LaMn_{0.9}Mg_{0.1}O_3$ (crosses), $LaMn_{0.8}Mg_{0.2}O_3$ (triangles), $LaMn_{0.7}Mg_{0.3}O_3$ (diamonds), $LaMn_{0.6}Mg_{0.4}O_3$ (circles), $LaMn_{0.5}Mg_{0.5}O_3$ (squares) and $CaMnO_3$ (solid line). Inset: Details of the pre-peak features after substracting the background.

is almost identical to that for $CaMnO_3$ (see Fig. 4) indicating a maximum Mn^{4+} oxidation state in this sample. This result nicely agrees with the previous crystallographic study and the chemical titration. In this way, we obtain a similar edge-position for $x=0.1$ and $x=0.2$ compounds in agreement with the oxygen excess of the former sample. It is worth distinguishing the kind of mixed valency present in $LaMn_{1-x}Mg_xO_3$ ($0.1\leqslant x\leqslant 0.4$) samples, i.e., a random distribution of Mn^{3+} and Mn^{4+} ions or an intermediate $Mn^{3.\eta+}$ state. The weighed addition of $LaMnO_3$ and $LaMn_{0.5}Mg_{0.5}O_3$ XANES spectra could reproduce the edge position of the spectra for the rest of the samples with intermediate compositions. However, it fails to reproduce the shape of the spectra because those for intermediate concentrations showed sharper absorption edges than the calculated from weighted

TABLE II. The relative energy shift of the absorption edge (respect to a Mn foil as reference, $E_0=6537.7$ eV) and the best fit results from the structural analysis of the first shell of the $LaMn_{1-x}Mg_xO_3$ series at the Mn K-edge. N is the coordination number, $R_{Mn\text{-}O}$ is the interatomic distance and σ^2 is the Debye-Waller factor. Numbers in parentheses are statistical errors in the last significant digit.

Sample	ΔE_0(eV)	N	$R_{Mn\text{-}O}$(Å)	$\sigma^2\times10^{-3}$(Å^2)
$LaMn_{0.5}Mg_{0.5}O_3$	16.8	6	1.89(1)	2.0(7)
$LaMn_{0.6}Mg_{0.4}O_3$	16.3	6	1.89(1)	3.9(7)
$LaMn_{0.7}Mg_{0.3}O_3$	15	6	1.90(1)	6.5(7)
$LaMn_{0.8}Mg_{0.2}O_3$	14.6	6	1.92(1)	7.9(6)
$LaMn_{0.9}Mg_{0.1}O_3$	14.6	6	1.93(1)	8.2(7)
$LaMnO_3$	13.2	4	1.92(1)	3.1(6)
		2	2.15(1)	3.5(7)

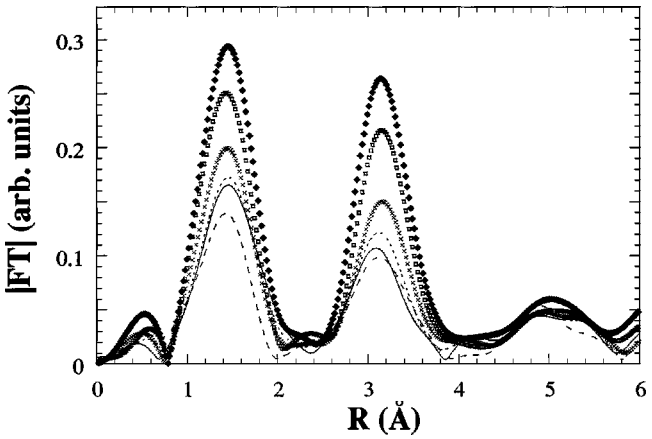

FIG. 5. Fourier transform for $LaMnO_3$ (broken line), $LaMn_{0.9}Mg_{0.1}O_3$ (solid line), $LaMn_{0.8}Mg_{0.2}O_3$ (dotted line), $LaMn_{0.7}Mg_{0.3}O_3$ (crosses), $LaMn_{0.6}Mg_{0.4}O_3$ (squares), $LaMn_{0.5}Mg_{0.5}O_3$ (diamonds).

addition of the reference ones. This result seems to point out to an intermediate $Mn^{3.\eta+}$ state as occur in related manganites.[25,28]

The XANES spectra also show broad resonances above the absorption edge, ascribed to multiple scattering effects, and weak pre-peak resonances at ~10 eV below the absorption edge. The pre-peak resonances show complicated structures. They are displayed in detail in the inset of Fig. 4 after subtracting the edge contribution. The pre-peak features are usually ascribed to $1s \rightarrow 3d$ transitions either allowed quadrupolar (very weak) or forbidden dipolar. The latter become allowed due to a strong mixing between 3*d* and 2*p* orbitals arising from the transition metal (Mn) and oxygen atoms, respectively. Some authors recently claim[29] that these pre-peaks in oxides arise from the mixing of *d*-states between neighboring Mn atoms through hybridization with the oxygen *p*-band. Then, the intensity of the pre-peaks is a measurement of the density of *d*-states from neighbor transition metal atoms. Our results seem to confirm this hypothesis. First, the intensity of the $CaMnO_3$ pre-peaks is higher than that for $LaMnO_3$, in agreement with the increase of Mn^{4+} near-neighbors with more empty 3*d*-states. Second, the $LaMn_{1-x}Mg_xO_3$ samples, instead, show less intensity in the pre-peak features in spite of the mixed valency state of the Mn atoms. Moreover, the intensity decreases with increasing the Mg-content. This finding is very likely to be related to the increase of Mg^{2+} ions (without 3*d* states) as near-neighbors of the MnO_6 octahedra. In particular, it is significant the comparison between $CaMnO_3$ and $LaMn_{0.5}Mg_{0.5}O_3$. Both samples have Mn^{4+} ions but in the latter case, the Mn is only surrounded by Mg^{2+} ions.

The room temperature EXAFS spectra were also measured for the $LaMn_{1-x}Mg_xO_3$ samples. Figure 5 shows the FT for the whole series compared to the undoped compound, $LaMnO_3$. All of the FT spectra show two strong peaks below 4 Å. The first one at around 1.5 Å (without the phase-shift correction) corresponds to the first coordination shell (Mn-O). The second peak, above 3 Å, is associated to the second shell with Mn-Mg(Mn), Mn-La and Mn-O contributions together with multiple scattering paths. The intensity of both

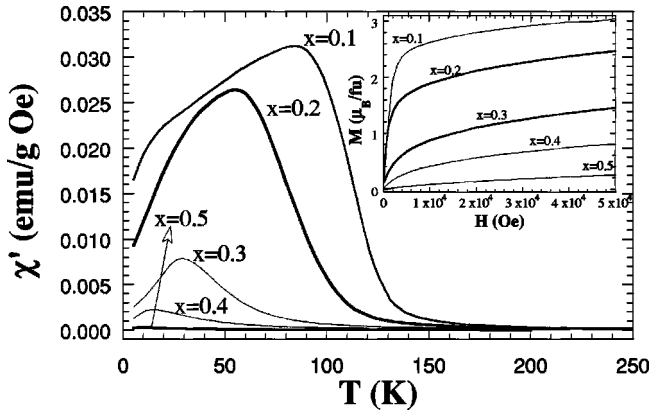

FIG. 6. The ac magnetic susceptibility for $LaMn_{1-x}Mg_xO_3$ samples. Inset: Isothermal magnetization curves at 5 K for the same samples.

peaks increases as the content of Mg does. This result can be understood in basis to the previous crystallographic study. Accordingly, the increase of both peaks is in agreement with the diminution of the orthorhombic distortion in the unit cell. For instance, the first coordination shell in $LaMnO_3$ is composed by three Mn-O distances (with a strong Jahn-Teller tetragonal distortion) whereas there is only one Mn-O distance for the rhombohedral $LaMn_{0.5}Mg_{0.5}O_3$. The rest of the samples exhibit the continuous evolution from the former to the latter compound.

The analysis of the first coordination shell was performed in the *R*-space (see Sec. II for details). The best-fit parameters are summarized in Table II. An average Mn-O distance is observed for all doped samples. Such a distance decreases as the content of Mg increases in agreement with the increase of Mn valency. A minimum value of 1.89 Å is found for $x = 0.4$ and $x = 0.5$ in accordance to typical values of Mn^{4+} oxides such as $CaMnO_3$.[25] The main structural effect along the series is expected to be in the Debye-Waller factor (σ^2) giving us information about the spread of Mn-O distances. The highest is the Mn valency the lowest is σ^2. This result agrees with the presence of regular MnO_6 octahedra in $x \geqslant 0.4$ samples. It is noteworthy that these samples exhibit a rhombohedral crystallographic cell. The trend of σ^2 in this series is similar to that observed in related manganites with intermediate Mn valency.[25] Nevertheless, the disorder induced by the addition of Mg into the Mn sublattice could also influence the σ^2 value in this system.

The Mn-O distances for $x = 0.4$ and 0.5 samples nicely agree with Sec. III A (see Fig. 3). The rest of the samples also show a good agreement with the diffraction results. In this case, it is worth realizing that EXAFS measured only the Mn-O contribution whereas the interatomic distances obtained from x-ray diffraction concerns both Mn-O and Mg -O distances (according to the existence of a solid solution).

C. Magnetic properties

Figure 6 shows the zero-field in-phase ac susceptibility (χ'_{ac}) for the whole series. The χ'_{ac} curves for $LaMn_{0.9}Mg_{0.1}O_3$ and $LaMn_{0.8}Mg_{0.2}O_3$ have strong anomalies

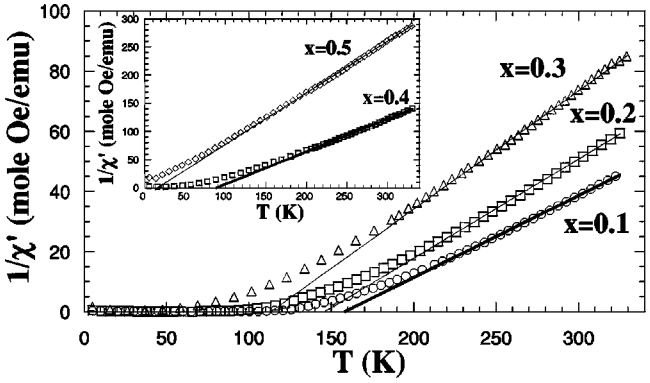

FIG. 7. Inverse of ac magnetic susceptibility vs temperature for $x \leqslant 0.3$. **Inset:** Inverse of ac magnetic susceptibility vs temperature for $x \geqslant 0.4$. The straight lines are the fits to a Curie-Weiss law from 200 up to 330 K. The regression of the linear fits were better than 0.9996 for all cases.

typical of long range ferromagnetic (FM) ordering. The Curie temperature (T_C) defined as the inflection point in the χ'_{ac} curves decreases as the content of Mg increases, in agreement[30] with the nonmagnetic character of Mg^{2+}. Below T_C, the χ'_{ac} of both samples decrease as temperature does. This behavior, characteristic of weak FM, might indicate the presence of a canted structure as found in other manganites.[2]

The rest of the samples ($x \geqslant 0.3$) show a peak at low temperatures in the χ'_{ac} curves. Hereafter, we denote the peak temperature as T_f. This fact is likely to be related to the lack of long-range FM ordering for samples with a high concentration of nonmagnetic Mg^{2+} ions. Both the height of T_f and its position decrease with increasing the content of Mg.

The inset of Fig. 6 shows the isothermal magnetization curves, $M(H)$, at 5 K for the whole series. All samples show spontaneous magnetization indicating the presence of FM interactions at 5 K. However, magnetic saturation is not achieved at 5 T in any case. The $M(H)$ curves have a positive slope at high magnetic fields that may be ascribed either to the presence of a canted structure ($x \leqslant 0.2$) or to a paramagnetic contribution. The spontaneous magnetization, or FM component, decreases as the Mg content increases. This result indicates that FM is weakened by the addition of the nonmagnetic Mg^{2+}. Although we cannot define a saturated magnetic moment, we have made use of the value of $M(H)$ at 5 T for the sake of comparison. We observed significant differences between the value of $M(H)$ at 5 T and the theoretical saturated magnetic moments. Moreover, this difference increases as the Mg content does. For instance, $M(H)$ at 5 T is 3.05 and 2.1 μ_B/fu for $LaMn_{0.9}Mg_{0.1}O_3$ and $LaMn_{0.8}Mg_{0.2}O_3$, respectively, whereas theoretical values (a spin-only contribution) would be 3.3 and 3.0 μ_B/fu, respectively. The discrepancy is even higher for the rest of the samples. This result also suggests the lack of FM ordering as Mg replaces Mn in the unit cell.

Figure 7 shows the $1/\chi'_{ac}$ vs temperature curves for the whole series. It is noteworthy that all samples obey the Curie-Weiss law at high temperatures, well above T_C ($x \leqslant 0.2$) or T_f ($x \geqslant 0.3$). The best-fit parameters are summarized in Table III together with the theoretical paramagnetic effective moments (ρ_{th}). The fits are also included in Fig. 7 and it is easy to note that all lines cut the positive x-axis indicating a preponderance of the FM interactions. The cut point (Weiss constant) decreases as x increases in agreement with a weakening of the FM interactions. The experimental paramagnetic effective moment (ρ_{eff}) also decreases with increasing x. Two contributions can account for this result. First, the increase of the nonmagnetic Mg^{2+} ions and second, the increase of the Mn^{4+}/Mn^{3+} ratio (diminution of $3d$ electrons) with increasing the Mg content. The ρ_{eff} are compared to ρ_{th} in Table III. The latter have been calculated considering a spin-only contribution and taking into account the Mn^{4+}/Mn^{3+} ratio deduced from the oxygen content (see Table I). There is a significant difference between ρ_{eff} and ρ_{th} values for samples with a low content of Mg. This discrepancy may be ascribed to the presence of short-range FM interactions above T_c as was observed in other manganites.[31] Such a discrepancy diminishes for samples with a high content of Mg and the experimental ρ_{eff} of $LaMn_{0.5}Mg_{0.5}O_3$ approaches the theoretical value.

The χ'_{ac} curves of Fig. 6 highlighted the lack of FM ordering for $x \geqslant 0.3$ samples. In order to gain insight into the magnetic properties of these samples, we have measured dc magnetization vs temperature curves at different magnetic fields. The measurements, displayed in Fig. 8, were carried out in Zero-Field Cooled (ZFC) and Field-Cooled (FC) conditions. Figure 8(b) shows the results for $x=0.4$. At low fields (0.1 kOe), both FC and ZFC curves have a peak at ~10 and ~14 K, respectively. Magnetic irreversibility begins at temperatures above these maxima. The increase of the field

TABLE III. Magnetic data from the fits of experimental ac susceptibility to the Curie Weiss law. C refers to Curie constant, θ to Weiss constant, ρ_{eff} is the experimental effective paramagnetic moment and ρ_{th} is the theoretical effective paramagnetic moment (spin-only). We consider $LaMn_{1-x}Mg_xO_{3\pm\delta}$ as a formula unit. Finally, T_C ($x \leqslant 0.2$) is the Curie temperature obtained from the inflection point of the χ'_{ac} (T) curves and T_f ($x \geqslant 0.3$) is the peak temperature of χ'_{ac} (T) curves measured at 9 Hz of the ac field.

Sample (x)	C (emuK/moleOe)	θ (K)	ρ_{eff} (μ_B/fu)	ρ_{th} (μ_B/fu)	T_C or T_f (K)
0.1	3.65	158.0	5.41	4.55	112
0.2	3.08	143.7	4.96	4.17	79
0.3	2.43	116.5	4.41	3.75	31.5
0.4	1.70	91.6	3.69	3.28	14
0.5	1.06	23.2	2.91	2.73	8.5

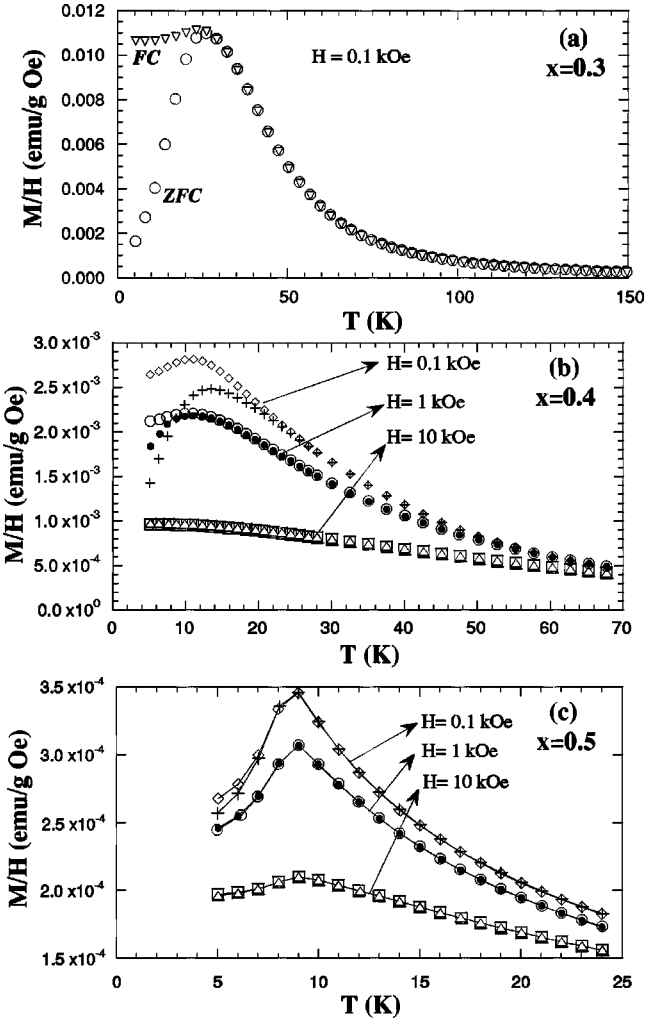

FIG. 8. Magnetization vs temperature curve after cooling the samples without an external magnetic field (ZFC branch) or cooling with the measuring field (FC branch) for $LaMn_{0.7}Mg_{0.3}O_3$ (a), $LaMn_{0.6}Mg_{0.4}O_3$ (b) and $LaMn_{0.5}Mg_{0.5}O_3$ (c).

(~1 kOe) has two effects: The height of the peak decreases and is shifted to a lower temperature. The irreversibility range also decreases and it begins at around the cusp of both curves. Finally, the peak is completely smoothed down at 10 kOe where FC and ZFC curves are identical. Small differences are observed in the other two samples. For instance, the magnetic irreversibility of $LaMn_{0.7}Mg_{0.3}O_3$, shown in Fig. 8(a), begins at the peak since the lower field-tested. The $LaMn_{0.5}Mg_{0.5}O_3$ instead, show a small irreversibility at temperatures below the peak that practically disappears at 1 kOe [Fig. 8(c)].

The divergence in the ZFC and FC curves is a feature ascribed to spin (or cluster)-glass behavior.[32,33] In order to ascertain it, the ac susceptibility at low temperature was also studied in detail for $x \geqslant 0.3$ samples. Figure 9 shows the temperature dependence of the ac susceptibility (in-phase component) at different frequencies of the alternating field. All these curves exhibit a clear peak at T_f. A dynamic behavior is deduced for the three samples. The height of the peak at T_f slightly decreases and it is shifted to higher temperatures with increasing the frequency of the ac field. This behavior is

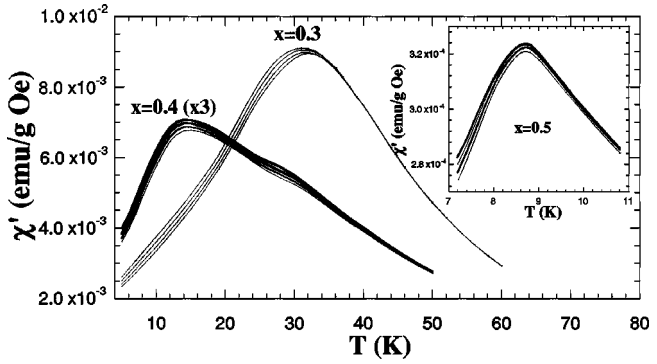

FIG. 9. Details of the ac susceptibility at low temperature and at different frequencies for $x=0.3$ and 0.4 (multiplied by 3). Inset: ac susceptibility curves for $x=0.5$. The frequencies of the ac field were (from left to right) 0.9, 9, 90 and 900 Hz.

observed at and below T_f for $x=0.3$ and 0.5. The $x=0.4$ sample instead shows a shoulder at higher temperature (~30 K) that also shows dynamic behavior. The out-of phase component of this sample also shows two peaks ascribed to these features (not shown here). Therefore, the χ'_{ac} curves at different frequencies converge at temperatures well above T_f in this case. This finding is likely to be related to the magnetic irreversibility observed in the dc magnetization (compare in Fig. 8 the different results between $x=0.4$ and the other two samples, for instance).

This dynamic behavior of the χ'_{ac} curves is also characteristic of spin (cluster)-glass systems. The frequency (υ) dependence of T_f is usually characterized by the term $\Delta T_f/(T_f \times \Delta \ln \upsilon)$. In the present series, this term decreases as the Mn content does. It ranges between 4.5×10^{-3} and 5×10^{-4}, values that address very well with canonical spin-glasses.[32,33] The frequency dependence of T_f, $T_f(\upsilon)$, cannot be fitted by an Arrhenius law in the whole series. They obey instead, a Vogel-Fulcher law,[32–34] $\upsilon = \upsilon_0 \exp[-E/K_B(T_f - T_O)]$. This empirical law is often done in treating the vitrification of real glasses but there is not agreement about the physical interpretation of the critical temperature, T_O, in the case of spin-glasses. Nevertheless, it is widely used in the magnetic studies of spin-glasses for the sake of comparison. Taking a value[34] of $\upsilon_0 = 10^{-13}$ s^{-1}, we have obtained reasonable values for T_O and E/K_B. T_O is 27, 13 and 8 K for $x=0.3$, 0.4 and 0.5 samples, respectively. The activation energy, E/K_B, values 100, 42 and 4 K for the same samples. The diminution of both parameters with increasing x is in agreement with a decrease in the number of frozen magnetic atoms.[34] Finally, we note that the dynamic behavior found in $LaMn_{1-x}Mg_xO_3$ ($x \geqslant 0.3$) is smaller than other manganites characterized as cluster-glasses. This may be a consequence of the role of Mg^{2+} ions that tend to form a double perovskite avoiding the gathering of Mn-clusters.

Our measurements confirm the presence of a spin-glass-like phase for $x \geqslant 0.3$ samples. This implies the presence of competitive interactions and randomness leading to magnetic frustration.[32] Both randomness and competitive interactions can easily be invoked for $x=0.3$. First, we have not detected a double perovskite structure for this sample (ordering of Mg^{2+} and $Mn^{3.7+}$ onto the B-sites) but the tendency of Mg^{2+}

to be surrounded by MnO_6 octahedra has to be taken into account. Second, competitive interactions are found in oxides with Mn in mixed valence. For example, considering an assembly of Mn^{3+} and Mn^{4+} ions as a rough approximation, either AFM (Mn^{4+}-O-Mn^{+4} or Mn^{3+}-O-Mn^{+3}) and FM (Mn^{4+}-O-Mn^{+3}) interactions are expected.[35]

A bit more difficult could be to understand the presence of competitive magnetic interactions in $x=0.5$. A perfect double perovskite with alternating Mg^{2+} and Mn^{4+} would result in isolated Mn^{4+} ions and a paramagnetic ground state would be expected. Several possibilities could account for this behavior. First, long-range superexchange interactions were invoked in the past to account for the magnetic ordering in related double perovskites.[36] Second, the presence of miss-site defects, quite common in double perovskites, could also allow the formation of Mn^{4+}-O-Mn^{4+} paths in this compound. In this case, it is worth noting that there is not spin glasses with only AFM interactions[32] so only miss-site defects are not enough to form competitive interactions. However, the presence of oxygen deficiency as a source for a bit of mixed-valence Mn could give rise to the presence of competitive interactions. The small oxygen deficiency indicated in Table I for this sample would agree with this hypothesis. Accordingly, the low value of T_f agrees with a very low amount of "magnetic impurities."

Finally, the $x=0.4$ sample shows particular features, namely two anomalies in the χ'_{ac} curves and a large ZFC-FC magnetic irreversibility at temperature above T_f. Chemical inhomogeneities cannot be discarded to explain these properties. However, such inhomogeneities could be intrinsic to the sample. We note that this sample has the structure typical of a double perovskite so part of Mn atoms must be located into the big "Mg-site." Bearing in mind the two crystallographic sites for Mn atoms, the two magnetic anomalies may arise from a bimodal distribution of magnetic clusters with different sizes. In such a case, the sample would be composed of clusters similar to the $x=0.5$ sample (regions with Mn almost isolated) and clusters similar to $x=0.3$ (neighborhood to the Mn located in the "Mg-site").

IV. CONCLUSIONS

The substitution of Mn with Mg in $LaMnO_3$ strongly affects the crystallographic and magnetic properties of the $LaMn_{1-x}Mg_xO_3$ system. There is not evidence of the reported substitution of La with Mg. In fact, the tested $La_{1-x}Mg_xMnO_3$ samples were multiphasic, $LaMn_{1-x}Mg_xO_3$ being the only perovskite phase (see the Appendix). No long range ordering of Mg and Mn atoms onto the B-site was detected for $x\leqslant 0.3$ samples. The crystal structure is orthorhombic without the periodic arrangement of tetragonal distorted MnO_6 octahedron (O′-structure) characteristic of the parent compound ($x=0$). Higher levels of replacing ($x\geqslant 0.4$) leads to an ordered arrangement of Mg and Mn atoms onto the B site giving rise to a double $ABB'O_6$ perovskite. We have detected two perovskite phases at room temperature in this concentration range: rhombohedral (main phase) and monoclinic (minority). This result is ascribed to a structural phase transition just around room temperature for both samples. Both samples are single phase at 77 K (monoclinic) and above room temperature (rhombohedral). The appearance of a rhombohedral cell is justified by the average decrease of the B-sublattice due to formation of Mn^{4+} whose small ionic radius has more effect on the B-size than the big Mg^{2+}.

XANES evidenced that the oxidation state of Mn continuously increases from +3 ($x=0$) up to +4 ($x=0.5$). Therefore, an intermediate valency of the Mn atom is observed for intermediate concentrations as occurs in $La_{1-x}Ca_xMnO_3$ samples.[28] According to the XANES results, EXAFS measurements showed a continuous decrease of the Mn-O distances with an increase in the content of Mg. There is not evidence of tetragonal distortion in the MnO_6 octahedron since the lowest substitution tested ($x=0.1$).

The σ^2 factors exhibit the same trend in both $LaMn_{1-x}Mg_xO_3$ and $La_{1-x}Ca_xMnO_3$ series. In fact, σ^2 has similar values for $CaMnO_3$ and $LaMn_{0.5}Mg_{0.5}O_3$. The rest of $LaMn_{1-x}Mg_xO_3$ samples show higher σ^2 values for the same nominal Mn valency. This finding may be ascribed to the disorder induced by the Mg substitution in the Mn sublattice.

Magnetic properties also change drastically. The occurrence of FM for $x\leqslant 0.2$ samples is ascribed to the mixed-valence state of Mn atoms as occurs in related manganites.[1] However, the insulating behavior of these samples[9,10] highlights, the importance of a perfect Mn sublattice to achieve the metallic FM state inferred from the double exchange mechanism.[37] The disorder induced by Mg is enough to localize carriers but it does not preclude the magnetic ordering. T_C diminishes with increasing x and for $x\geqslant 0.3$ a random magnetic system is observed at low temperatures. The loss of FM ordering can be understood in terms of two combined effects. First, the increase of formal Mn-valency giving rise to competitive interactions and second, the disorder induced by substituting Mg for Mn in spite of the tendency to develop a selective occupation onto the perovskite B-sites. The spin-glass transition is developed at lower temperatures as the Mn content decreases in agreement with a diminution of the number and size of magnetic clusters. The spin-glasses were characterized and $T_f(\upsilon)$ of the three samples follows a Vogel-Fulchar law with fit-parameters similar to other spin-glass systems.

ACKNOWLEDGMENTS

This work was supported by CICyT (Spain) Project No. MAT02/01221 and DGA. We acknowledge the ESRF for beam time allocation. We are also indebted to the BM29 staff for the technical support in the XAS measurements.

APPENDIX: IS IT POSSIBLE TO SUBSTITUTE Mg FOR La IN $LaMnO_3$?

Recent studies[11–14] claim for the substitution of Mg for La in the perovskite lattice. This finding was a subject of controversy[38] that keeps on to date. The ceramic procedure reported to prepare $La_{1-x}Mg_xMnO_3$ is very similar to the synthetic route used in this work so a partial distribution of Mg^{2+} ions onto both sites would influence the physical prop-

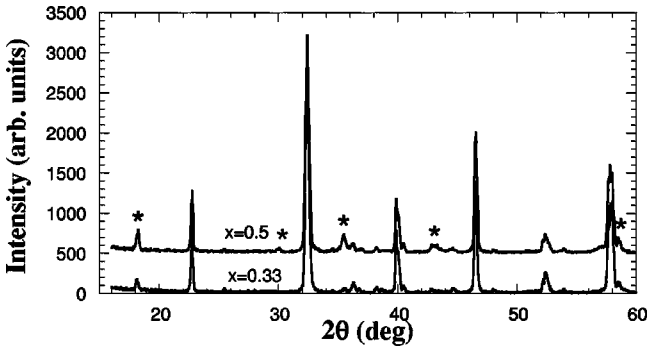

FIG. 10. Details of the x-ray patterns for $La_{0.67}Mg_{0.33}MnO_3$ and $La_{0.5}Mg_{0.5}MnO_3$ at room temperature.

erties, strongly. Nevertheless, this kind of replacement is quite surprising considering that there are not examples of solid solutions between Mg and La oxides in the literature[39] while there is a lot of Mg and Mn mixed oxides forming solid solutions.[40,41] First of all, Mg^{2+} is too small for the 12-fold coordinated A-site in the perovskite cell. Even, there is not a tabulated ionic radius for 9-fold coordinated Mg^{2+} with oxygen atoms.[23] Moreover, other ions with similar size form competitive ABO_3 phases[42] such as $InMnO_3$ (note the similar ionic sizes for 8-coordinated In^{3+} and Mg^{2+} that are 0.92 and 0.89 Å, respectively). Finally, if Mg^{2+} replaced La^{3+} in the perovskite cell, the easy preparation of $LaMn_{1-x}Mg_xO_3$ phases would be quite surprising without the apparent segregation of secondary phases arising from the partial substitution of La.

In order to gain insight into the site-preference of Mg^{2+} ions, we attempted to prepare several $La_{1-x}Mg_xMnO_3$ samples ($x=0.33,0.5$) following the reported synthesis.[11–14] We have never found single phases in our samples though the main phase is a perovskite. Figure 10 shows the x-ray patterns for both samples. Impurity peaks are clearly visible and according to the binary MgO-Mn_2O_3 phase diagram,[41] they can be ascribed to the presence of spinel (Mg_2MnO_4) and Hausmanite-like ($Mg_{1-x}Mn_{2+x}O_4$) phases. Concerning the perovskite phase, we were not able to reproduce the previous results.[13,14] Our patterns can hardly be indexed in the frame of an orthorhombic phase with the large distortion reported elsewhere.[14] A detailed inspection of the patterns evidences the presence of two perovskite phases, orthorhombic and rhombohedral.

Secondly, Rietveld analysis clearly shows that Mg does not enter into the La-site. Figure 11(a) shows the best refinement for $La_{0.67}Mg_{0.33}MnO_3$ using a single orthorhombic perovskite phase. Convergence is not reached, not only due to the additional peaks from secondary phases but also to the strong discrepancy in the intensity of several perovskite peaks. Such a discrepancy will disappear considering that Mg replaces Mn in these samples. A conclusion results evident. If we always substituted Mn for Mg, we would have an excess of Mn/Mg in the $La_{1-x}Mg_xMnO_3$ samples giving rise to the mentioned secondary phases. We were successful in

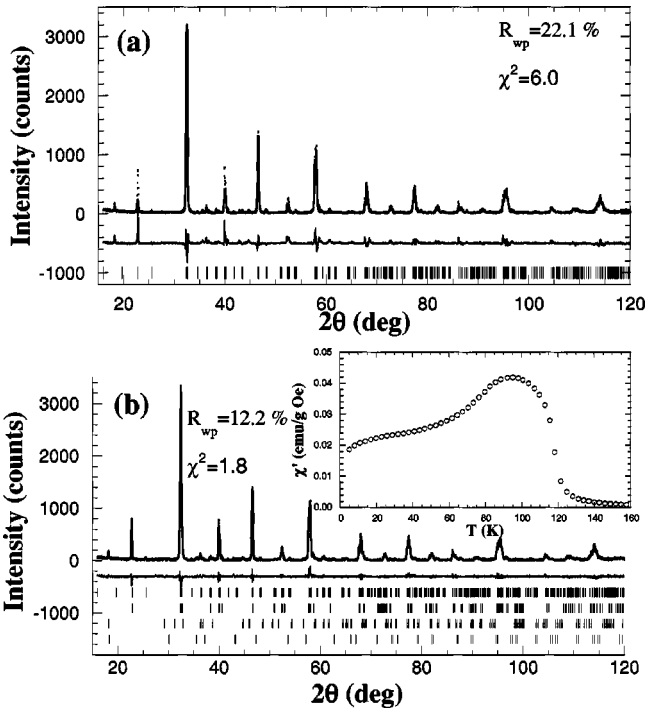

FIG. 11. Profile refinement of the $La_{0.67}Mg_{0.33}MnO_3$ x-ray pattern considering (a) a single orthorhombic perovskite phase; (b) four phases: *Pbnm* and $R\bar{3}c$ perovskites with a Mn/Mg solid solution, cubic spinel Mg_2MnO_4 and hausmanite $MgMn_2O_4$. **Inset:** the ac magnetic susceptibility for $La_{0.67}Mg_{0.33}MnO_3$. Reliability factors indicated in both figures are defined in Ref. 15.

refining our x-ray patterns by using four phases: *Pbnm* perovskite, $R\bar{3}c$ perovskite, $MgMn_2O_4$ and Mg_2MnO_4. The Mn/Mg ratio in the perovskite phases was fixed to the starting value and the final refinement for the nominal $La_{0.67}Mg_{0.33}MnO_3$ is shown in Fig. 11(b).

On the other hand, the inset of Fig. 11(b) shows the ac magnetic susceptibility of $La_{0.67}Mg_{0.33}MnO_3$ that correlates quite well with the reported in Ref. 12 for the same nominal sample. These results indicate that the properties ascribed to $La_{1-x}Mg_xMnO_3$ single phases might be due to a mixture of phases. In the same way, the substitution of Mg for Mn can go unnoticed for low doping ratio due to the formation of La vacancies, the so-called self-doping.[38]

Finally, we have not detected the presence of superstructure peaks arising from the Mn/Mg ordering in these perovskite phases justifying the use of *Pbnm* and $R\bar{3}c$ space groups. This is in agreement with the relative low Mg/Mn ratio but, surprisingly, a rhombohedral phase is now observed for $Mg/Mn \sim 0.33$ while in section III A, we observed a single orthorhombic phase for $Mg/Mn \sim 0.43$. This fact is most likely to be related to differences in the oxygen content between both series due to the different sintering temperature (lower for $La_{1-x}Mg_xMnO_3$ samples). It is well known that oxygen excess favors the appearing of rhombohedral phases in the $LaMnO_{3+\delta}$ system.[43]

*Corresponding author: J. Blasco, I.C.M.A., Departamento de Física de la Materia Condensada, C.S.I.C.-Universidad de Zaragoza, Pedro Cerbuna, 12, 50009 Zaragoza, Spain. Electronic address: jbc@unizar.es; Fax:+34-976-761229.

[1] J. M. D. Coey, M. Viret, and S. Von Molnar, Adv. Phys. **48**, 167 (1999).
[2] J. Blasco, J. García, J. Campo, M. C. Sánchez, and G. Subías, Phys. Rev. B **66**, 174431 (2002).
[3] M. C. Sánchez, G. Subías, J. García, and J. Blasco, Phys. Scr. (to be published).
[4] K. H. Ahn, X. W. Wu, K. Liu, and C. L. Chen, Phys. Rev. B **54**, 15299 (1996).
[5] Q. Huang, Z. W. Li, J. Li, and C. K. Ong, J. Phys.: Condens. Matter **13**, 4033 (2001).
[6] V. P. S. Awana, E. Schmitt, E. Gmelin, A. Gupta, A. Sedky, V. Narlikar, O. F. de Lima, C. A. Cardoso, S. K. Malik, and W. B. Yelon, J. Appl. Phys. **87**, 5034 (2000).
[7] G. Blasse, J. Phys. Chem. Solids **26**, 1969 (1965).
[8] G. Saracco, F. Geobaldo, and G. Baldi, Appl. Catal., B **20**, 277 (1999).
[9] T. R. N. Kutty, and J. Philip, J. Phys.: Condens. Matter **12**, 7747 (2000).
[10] J. Philip and T. R. N. Kutty, Mater. Chem. Phys. **73**, 220 (2002); Appl. Phys. Lett. **79**, 209 (2001).
[11] J. H. Zhao, T. Song, H. P. Kunkel, X. Z. Zhou, R. M. Roshko, and G. Williams, J. Clin. Eng. **12**, 6903 (2000).
[12] X. Z. Zhou, H. P. Kunkel, J. H. Zhao, P. A. Stampe, and G. Williams, Phys. Rev. B **56**, R12714 (1997).
[13] J. H. Zhao, H. P. Kunkel, X. Z. Zhou, and G. Williams, J. Phys.: Condens. Matter **13**, 9349 (2001).
[14] J. H. Zhao, H. P. Kunkel, X. Z. Zhou, and G. Williams, Phys. Rev. B **66**, 184428 (2002).
[15] J. L. Rodríguez-Carvajal, Phys. Status Solidi B **55**, 191 (1992); J. L. Rodríguez-Carvajal and T. Roisnel, available at http://www-llb.cea.fr/fullweb
[16] E. A. Stern, H. Newville, B. Ravel, Y. Yaroby, and D. Haskel, Physica B **208&209**, 117 (1995); http://FEFF.phys.washington.edu
[17] A. L. Ankudinov andJ. J. Rehr, Phys. Rev. B **62**, 2437 (2000); http://leonardo.phys.washington.edu/feff/
[18] J. A. M. Van Roosmalen and E. H. P. Cordfunke, J. Solid State Chem. **93**, 212 (1991).
[19] J. Blasco,J. García, M. C. Sánchez, J. Campo, G. Subías, and J. Pérez-Cacho, Eur. Phys. J. B **30**, 469 (2002).
[20] P. M. Woodward, Acta Crystallogr., Sect. B: Struct. Sci. **53**, 32 (1997).
[21] J. Blasco,M. C. Sánchez, J. Pérez-Cacho, J. García, G. Subías, and J. Campo, J. Phys. Chem. Solids **63**, 781 (2002).
[22] A. M. Glazer, Acta Crystallogr., Sect. A: Cryst. Phys., Diffr., Theor. Gen. Crystallogr. **31** 756 (1975).
[23] R. D. Shannon, Acta Crystallogr., Sect. A: Cryst. Phys., Diffr., Theor. Gen. Crystallogr. **32** 751 (1976).
[24] C. Ritter, M. R. Ibarra, L. Morellón, J. Blasco, J. García, and J. M. De Teresa, J. Phys.: Condens. Matter **12**, 8295 (2000).
[25] J. García, M. C. Sánchez, G. Subías, and J. Blasco, J. Clin. Eng. **13**, 3229 (2001); F. Bridges, C. H. Booth, M. Anderson, G. H. Kwei, J. J. Neumeier, J. Snyder, J. Mitchell, J. S. Gardner, and E. Brosha, Phys. Rev. B **63**, 214405 (2001).
[26] M. C. Sánchez, J. García, J. Blasco, G. Subías, and J. Pérez-Cacho, Phys. Rev. B **65**, 144409 (2002).
[27] J. B. Goodenough, A. Wold, R. J. Arnott, and N. Menyuk, Phys. Rev. **124**, 373 (1961).
[28] G. Subías, J. García, M. G. Proietti, and J. Blasco, Phys. Rev. B **56**, 8183 (1997).
[29] Z. Y. Wu, D. C. Xian, C. R. Natoli, A. Marcelli, E. Paris, and A. Mottana, Appl. Phys. Lett. **79**, 1918 (2001).
[30] S. Hebert, C. Martin, A. Maignan, R. Retoux, M. Hervieu, N. Nguyen, and B. Raveau, Phys. Rev. B **65**, 104420 (2002).
[31] J. M. de Teresa, M. R. Ibarra, P. A. Algarabel, C. Ritter, C. Marquina, J. Blasco, J. García, and A. del Moral Nature (London) **386**, 256 (1997).
[32] J. A. Mydosh, *Spin Glasses* (Taylor & Francis, London, 1993).
[33] C. Y. Huang, J. Magn. Magn. Mater. **51**, 1 (1985).
[34] J. L. Tholence, Solid State Commun. **88**, 917 (1993).
[35] J. B. Goodenough, J. Phys. Chem. Solids **6**, 287 (1958); J. Kanamori, *ibid.* **10**, 87 (1959).
[36] G. Blasse, Philips Res. Rep. **20**, 327 (1965).
[37] C. Zener, Phys. Rev. **82**, 403 (1951).
[38] V. L. J. Joly, P. A. Joy, and S. K. Date, J. Phys.: Condens. Matter **13**, 6433 (2001).
[39] A. Rabenau, Z. Anorg. Allg. Chem. **288**, 221 (1956).
[40] P. V. Riboud and A. Muan, J. Am. Ceram. Soc. **46**, 33 (1963).
[41] V. P. Barkhatov, Y. V. Golikov, A. G. Zalazinskii, V. F. Balakirev, and G. I. Chufarov, Dokl. Chem. **252**, 370 (1980).
[42] D. M. Giaquinta and H. C. zur Loye, Chem. Mater. **6**, 365 (1994).
[43] C. Ritter, M. R. Ibarra, J. M. de Teresa, P. A. Algarabel, C. Marquina, J. Blasco, J. García, S. Oseroff, and S-W. Cheong, Phys. Rev. B **56**, 8902 (1997).